Hands-on quantum sensing with NV − centers in diamond

J. L. Sánchez Toural, V. Marzoa, R. Bernardo-Gavito, J. L. Pau, D. Granados

Hands-on quantum sensing with NV^- centers in diamond

J. L. Sánchez Toural*, V. Marzoa*, R. Bernardo-Gavito*, J. L. Pau** and D. Granados*

* IMDEA-Nanociencia, ** UAM. 28049 Madrid, Spain

I. Abstract

The physical properties of diamond crystals, such as color or electrical conductivity, can be controlled via impurities. In particular, when doped with nitrogen and under certain conditions, optically active nitrogen-vacany centers (NV) can be induced.

The center is an outstanding quantum spin system that enables, under ambient conditions, optical initialization, readout, and coherent microwave control with applications in sensing and quantum information.

Under optical and radio frequency excitation, the Zeeman splitting of the degenerate states allows the quantitative measurement of external magnetic fields with high sensitivity.

This study provides a pedagogical introduction to the properties of the NV centers as well as a step-by-step process to develop and test, a simple magnetic quantum sensor based on color centers with large potential for the development of highly compact multi-sensor systems.

Keywords: Quantum sensing. Diamond. Magnetometry at room temperature. Color centers. NV centers. Microwaves.

II. Introduction

The name diamond comes from the Greek *adamantem* which means invincible. Diamond is an electrical insulator whose strong covalent bonds make it a material with extraordinary hardness, broadband optical transparency and extremely high thermal conductivity. In addition, it can withstand large electric fields and, when doped, behaves like a semiconductor.

Diamonds are associated with the idea of perfection. However they are rarely perfect and lattice irregularities or impurities are very common.

Artificial diamonds can be produced artificially. The nature and density of impurities can be controlled during or after their growth. This alters their physical properties, such as color or electrical conductivity. Optically active defects are called color centers or NV centers.

In the NV color center, a nitrogen atom substitutes a carbon atom and a vacancy, in one of four adjacent positions, replaces another carbon atom. In this configuration, one electron is unpaired and remains trapped inside the vacancy. The center is charged negatively when it captures an additional electron, usually from a nitrogen atom donor in the lattice. The spin state of the two electrons quantum system, can be controlled using microwave pulses and optically addressed by measuring the photoluminescence [1].

All this, together with the long coherence time of the quantum state, and possibility of working at room temperature, makes them an ideal physical platform for the development of a magnetic sensor, with unprecedented performance.

The spin orientation of the two electrons trapped inside the center is aligned with the axis of symmetry (the line joining the vacancy and the nitrogen).

Under $532\ nm$ laser light illumination pulse, the center fluoresces emitting a photon in the red spectrum. Exciting with microwaves, the fluorescence changes in such a way that it is possible to determine the external magnetic field [2].

Current technologies providing a high magnetic sensitivity such as optical pumped magnetometry (OPM) [3], superconducting quantum interference devices (SQUID) [4], microelectromechanical systems (MEMS) [5] or magnetic resonance force microscopy (MRFM) [6] are highly successful technologies that have made possible the measurement of the magnetic field generated by neuronal activity with great precision. These systems have been previously described and compared [7].

A SQUID is based on superconducting loops containing Josephson junctions [9]. It is a very sensitive magnetometer used to measure extremely small magnetic fields, sensitive enough to measure fields as low as $5 \times 10^{-14}\ T$ with a noise equivalent field of about $3\ fT \cdot Hz^{-1/2}$. For the sake of comparison, it is important to notice that a common small neodymium magnet produces a magnetic field of about $10^{-2}\ T$, and neural activity in animals produces magnetic fields between $10^{-9}\ T$ and $10^{-6}\ T$. Spin exchange relaxation-free (SERF) magnetometers measure magnetic fields by using lasers to detect the interaction of the magnetic field with alkali metal atoms in a vapor. They are potentially more sensitive and do not require cryogenic refrigeration but are orders of magnitude larger in size ($1\ cm^3$) and must be operated in a near-zero magnetic field.

SQUID requires cryogenics, OPM reduces the sensitivity when the device reduces its dimension [10] due to the atomic collisions that alter the spin. These technologies show limitations for miniaturization, since either they require special conditions and bulky instrumentation or their temporal resolution decreases when trying to reduce their dimensions.

The quantum state of a color center in diamond can be read out optically because the fluorescence is spin-dependent, allowing its use in high-precision magnetometry at room temperature [11] [12]. Its properties have demonstrated temporal resolution [13] and ultra-high sensitivity [14] to measure fields as low as $10^{-12}\ T$ [15] while allowing device miniaturization down to millimeter, micrometer and even nanoscale.

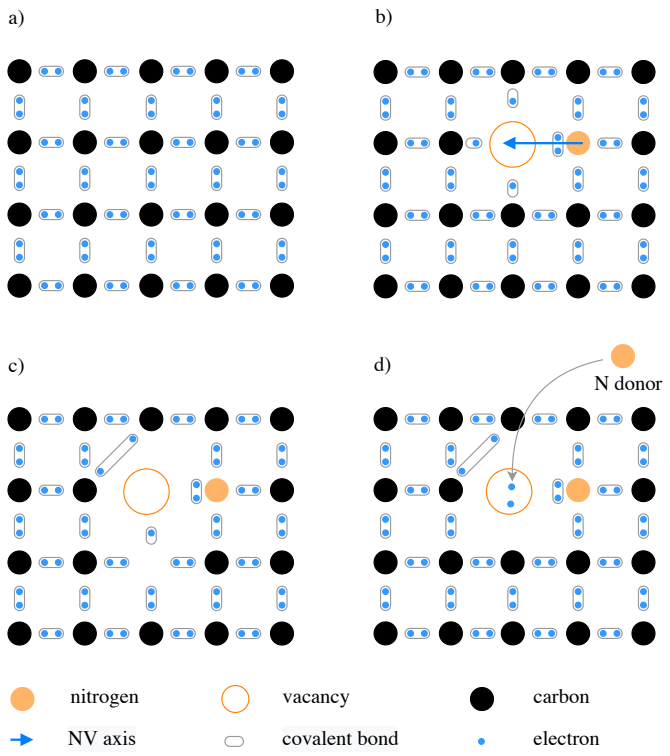

Figure II.1. Simplified, flat representation of the diamond lattice (a), a missing carbon atom, or vacancy, and the nearest neighbor, a substitutional nitrogen atom, create the NV center where the axis aligns the nitrogen atom with the vacancy, in one of four possible orientations (b), the nitrogen atom has five electrons in the valence band, three of them form three covalent bonds with the three neighbor carbon atoms, leaving a lone pair. From the carbon atoms surrounding the vacancy, three electrons from dangling bonds are also part of the center, one remains unpaired and the other two form a covalent bond (c). A total of five electrons leads to the neutral NV^0state which does not exhibit the magnetic activity as the negative charge state NV^- does. When the center captures a sixth electron [8], normally from another nitrogen atom donor in the lattice, the center is charged negatively and shows the expected behavior useful in magnetometry.

The crystal structure of diamond consists of tetrahedral covalent bonds between an atom and its four nearest neighbors, linked in a face-centered cubic Bravais lattice. This strongly bonded, tightly packed, dense and rigid structure gives rise to its outstanding properties.

A NV center [16] is a point defect in diamond with an axial, trigonal C_{3v}[17] symmetry [18] (three vertical reflection planes and two 120º rotations about the Z axis), caused by a nitrogen impurity. The center has three possible configurations, a positive charge NV^+, a neutral NV^0 (Figure II.1 a) and a negative charge NV^-(Figure II.1 d). These states have been well studied, NV^+ is non-fluorescent, NV^0 [19] [20] has only one electron unpaired, is paramagnetic and the luminescence intensity is lower than in the case of NV^-. The NV^- occurs when the center captures an additional electron, normally from a nitrogen donor in the lattice, and they form a pair with an integer quantum spin number of 0 or ± 1, and it is the one used for magnetometry [21].

The electronic structure of the center consists of a triplet ground state, a triplet excited state and two singlet states [22]. In the singlet state the spins are anti-aligned (up-down or down-up with $m_s = 0$). In the triplet state, the spins can be aligned (up-up with $m_s = +1$ or down-down with $m_s = -1$) or anti-aligned. The state with the spins aligned is degenerated and requires more energy due to the electron-electron magnetic interaction.

Magnetometry under ambient conditions with color centers in diamond is based on the optical measurement of the eigenvalues of the two spin Hamiltonian of the electrons trapped in the center under the application of an external magnetic field. The measurement can be performed optically because the $m_s = \pm 1$ degenerated states preferentially follow a non-radiative path through the metastable singlet states, resulting in a reduction in the observed photoluminescence [23] compared to that corresponding to the $m_s = 0$ state. Spin state initialization [24] is achieved by applying properly tuned laser light, which causes optical pumping to the $m_s = 0$ state. The microwave radiation at the resonance frequency populates the $m_s = \pm 1$ states that, under an external magnetic field, will split giving rise to a decrease in the PL observed at the resonance frequencies.

If the center is shined with a laser light (we used a $532\,nm$ or $2.33\ eV$, argon-ion laser), the electrons are excited from the ground to the excited state, where these transitions are predominantly spin conserving. The electrons immediately decay to the ground state and emitting a photon of a lower frequency (red color), this photoluminescence (PL) is more intense when the center is in the $m_s = 0$ state because the transition is closed (from $m_s = 0$ ground state to $m_s = 0$ excited state and then, back again to $m_s = 0$ ground state). In the case of $m_s = \pm 1$ the excitement conserves the spin but not the decay because one of the electrons flips and the state changes to $m_s = 0$, decaying through the metastable singlet states and emitting a photon in an infrared frequency [25], and therefore reducing the observed PL.

In a continuous optical excitation shining with a compact laser diode module ($532\,nm$) [26], all the electron population, initially in the $m_s = \pm 1$ state, is pumped to the $m_s = 0$ state, so this is the method to initialize the system, all the electrons set on the $m_s = 0$ state.

At this situation, it is not possible to observe the effect of an external magnetic field on the PL because the degenerated states $m_s = \pm 1$, are not populated. Applying a microwave radiation at the 2.87 GHz resonance frequency, the $m_s = \pm 1$ ground states are populated again allowing the excitement to the $m_s = \pm 1$ excited states and the subsequent decay through the non-radiative route showing a decrease in the PL.

Under this continuous microwave radiation, applying an external magnetic field with strength B_0, the magnetic moment of the electron aligns itself either antiparallel ($m_s = -1$) to the magnetic field component corresponding to the NV axis, with a specific energy level, or parallel ($m_s = +1$) with a different energy, due to the Zeeman shift of the spin sublevels. Therefore, now, the PL decreases at two different resonance frequencies. This separation of the sub-levels is linear and

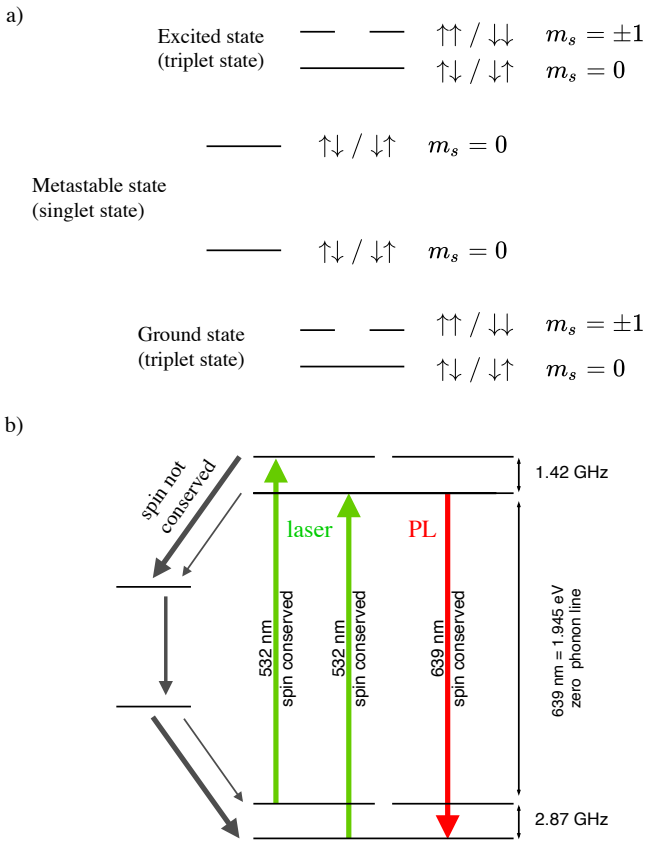

Figure II.2. Energy landscape of the NV^-center. Ground and excited states are split by spin interaction into a triplet. The electron is a fermion, its spin quantum number has a magnitude of $s = 1/2$ and two possible magnetic component $m_s = \pm 1/2$. The two electrons in the NV^-center exist in a triplet state: one state when electrons have opposite spins and $m_s = 0$, and two states when electrons have the spin pointing to same direction, (↑↑) or (↓↓), and $m_s = \pm 1$, in this case, the energy of the system is higher and the state is degenerated (a). The excitation (green arrows in the picture) conserves the spin and also the decay from $m_s = 0$ excited to $m_s = 0$ ground, however, when the center state is $m_s = \pm 1$ excited, one of the electrons flips and the state changes to $m_s = 0$ following (preferentially) a non radiative path through the metastable singlet states. The decay from $m_s = 0$ happens with the emission of a 639 nm (red arrow in the picture) photon corresponding to the zero phonon line (ZPL) and the decay from $m_s = \pm 1$ with the emission of a 1042 nm (infrared, black arrows in the picture), decreasing the observed PL intensity. Finally, the difference in energy between $m_s = 0$ and the degenerated states in the ground and excited states, with zero field splitting, corresponds to 2.87 GHz and 1.42 GHz respectively.

proportional to the applied magnetic field component corresponding to the NV axis and produces a decrease in the observed PL at those frequencies. Increasing the magnetic field and due to the hyperfine structure and different orientations of different NV centers, other levels are also split and different dips on the PL are observed.

III. Materials and Methods

A. Experimental Characterization

Color centers in diamond can be characterized experimentally using [27] [28] optically detected magnetic resonance (ODMR) or electron spin resonance (ESR) techniques together with the photoluminescence signal emitted during the relaxation of an excited state to its ground state. In this study, ODMR is used for the characterization of the color centers in diamond.

The experiments have been performed using two samples of commercially available synthetic Ib diamonds from element6 vendor [29], a polycrystalline diamond and a single crystal. These samples are grown by the High Pressure High Temperature (HPHT) synthesis processes. Throughout this research and for all experiments, the luminescence has been studied using an ensemble of NV^- centers in a polycrystalline and a single crystal diamonds where each NV^- axis is randomly oriented in all four possible directions.

It is important, for nanoscale applications, that the centers are located as close to the surface as possible. Type Ib diamonds are artificially fabricated [30] to contain up to 500 ppm nitrogen, absorb green light, and are dark yellow or brown in color. The samples used in our investigation have a central NV concentration of around 1 ppm.

With the sensor as the final target, the first step is the characterization of the two diamonds, developed for quantum sensing purposes. Both samples, the polycrystalline and the single crystal, have been characterized under ambient conditions using an argon ion laser at 40 μW power (Figure III.1) and 488 nm wavelength, in a low vibration optical setup, achieving almost identical results in PL intensity and peaks observed.

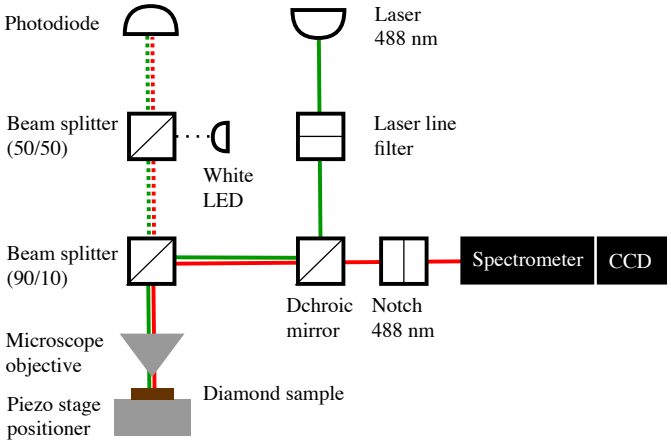

Figure III.1. Experimental setup used for the characterization of the samples. It includes a 488 nm laser source, a piezo-positioner, a confocal microscope, a dichroic mirror (94 : 06), a 488 nm long pass filter (notch), a beam splitter (90 : 10) a CCD camera, a spectrometer and other optical elements as shown in the diagram. The laser power source is 40 μW which is partially absorbed by the dichroic mirror and the splitter, reducing the power incident on the sample to 11.25 μW.

The PL intensity is linear to the excitation power, and due to the vibrational and rotational effects on atomic levels, it is not emitted at a single wavelength but in a range from 600 nm to 800 nm. The photoluminescence spectra (Figure III.2) shows the four characteristic frequency peaks: the NV^- zero phonon line (ZPL) at 639 nm, the NV^0 ZPL at 576 nm and the wide phonon sideband with two visible peaks at

662 nm and 684 nm [27]. A small Raman peak corresponding to the vibration of the sp3 (tetrahedral) diamond lattice was also identified. From Figure A.1 is deduced the ensemble of NV centers in both crystals are very similar and produce also a very similar luminescence.

The mentioned zero-phonon line and the phonon sidebands constitute the spectra of the single color centers in diamond absorbing and emitting light. For the ensemble of color centers, each NV center contributes with a zero-phonon line and a phonon sideband to the total absorption and emission spectra which is considered not homogeneously broadened because each NV center is surrounded by a different environment in the lattice which modifies in a different way the energy required for an electronic transition, shifting and overlapping each zero phonon and vibrionic phonon sideband positions [31].

The zero-phonon line is located at a frequency determined by the energy gap between the NV center ground and excited state and also determined by the local environment. The phonon sideband is shifted to a higher frequency in absorption and to a lower frequency in fluorescence with peacks showed in Figure A.1.

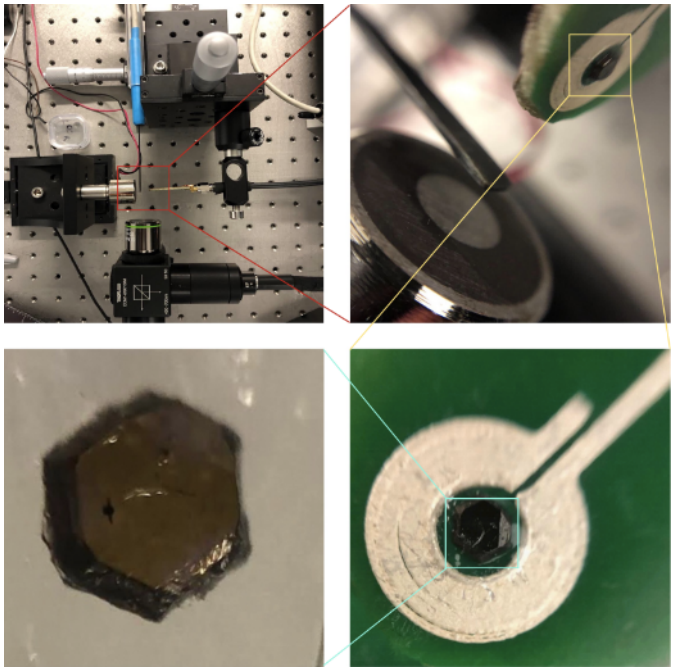

Figure III.2. View of the experimental setup at different levels of detail. The bottom left picture shows a zoom image of the diamond sample.

B. Optical initialization and read out

Because the magnetic field is detected optically through the splitting of the degenerated states due to the Zeeman effect, the next step in the process requires the $m_s = \pm 1$ center state populated. For that purpose the setup is extended adding a microwave source and a resonator.

As shown before, by continuously applying laser light (532 nm diode), the electrons in the centers are pumped to the $m_s = 0$ ground state (Figure II.2). Applying a resonant microwave field with an energy of 2.87 GHz, corresponding to the gap between the quantum levels $m_s = 0$ and $m_s = \pm 1$, the electrons in the center are excited to the $m_s = \pm 1$ state.

The comparative measurement of the 1042 nm transition, applying or not the resonant microwave field under continuous laser excitation, allows the detection of the PL attenuation, due to the greater absorption in the infrared frequency that occurs in the transition between the singlet states as well as the long coherence time of those singlet states (NV centers inhomogeneous spin relaxation time was assessed to be in the order of 300 ns, [32] [33]). When the microwave field is retired, the electrons return to the $m_s = 0$ state and therefore that transition does not take place, resulting in an increase in the photoluminescence.

To irradiate the diamond with microwaves pulses, the research team manufactured a resonator with the topology and characteristics described in Figure III.3, based on a previous design by Man Zhao et al. [34] and the study of Eisuke Abe et al. [35] by silver printing on a PCB using a Voltera V-One PCB printer [36].

The diamond sits on top of the resonator (not interrupting the laser light source or the objective) and generates a spatially uniform and concentrated field over an area of approximately 1 mm^2 with a resonance frequency of 2.87 GHz and a bandwidth of 100 MHz permitting to work with different resonances generated by the hyperfine structure.

C. Photoluminescence intensity in proportion to the applied microwave frequency

The new setup (Figure III.4-a) includes a microwave source, a spectrometer and a computer to process the signal, allowed us to visualize the effect of the microwaves in the PL. For that study we programmed the microwave (MW) source to sweep [37] in a range of frequencies from 2.7 GHz to 3.0 GHz (10 MHz step; 5.0 dBm constant power; 26 seconds sweep duration) and a code to integrate the total luminescence detected by the spectrometer per time unit (100 ms integration time).

As predicted by the theory we observed a dip right at the resonance frequency of 2.87 GHz. Under the laser beam (532 nm), the two electrons in the color center, are excited from the $m_s = 0$ ground state to the $m_s = 0$ excited state and then recombined again to the $m_s = 0$ ground state. The microwaves have no effect excepting for the resonance frequency. At this frequency, the electrons absorb the energy from the MW pulse and populate the $m_s = \pm 1$ ground state, from that, the laser beam excites them to the $m_s = \pm 1$ excited state to finally decay through the spin nonconservative and no radiative path across the metastable states, resulting in a reduced fluorescence signal (Figure III.5 a).

At this point, the research team was in conditions to move forward and explore the effect of the magnetic field in the photoluminescence.

D. PL under an external magnetic field

The spin-triplet ground state has a zero field splitting at 2.87 GHz between $m_s = 0$ and $m_s = \pm 1$ sublevels, splitting

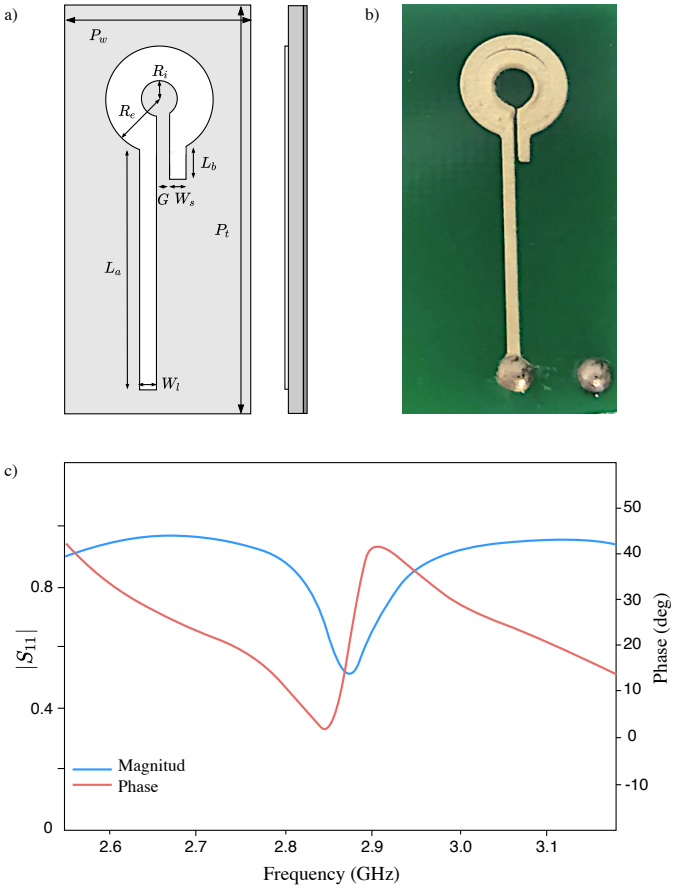

Figure III.3. The flat ring resonator is made up of a radiating patch, a dielectric substrate, and a grounding plate (b). The radiating ring structure was printed with silver on a substrate 1.3 mm PCB flat laminated composite substrate, made from a non-conductive material, and the grounding plate, a 0.08 mm thick copper foild. a) $P_w = 10.2$ mm and $P_l = 30$ mm are the PCB width and length respectively. The geometric dimensions (mm) of the resonator are: $L_a = 16$, $L_b = 2.1$, $W_l = 0.5$ $W_s = 0.5$, and $G = 0.2$. The inner and outer radius of the ring are: $R_i = 1.3$ mm and $R_e = 3.7$ mm respectively. The scattering, or S parameter, is depicted in d), S_{11} is the resonator reflection coefficient, it is a ratio and therefore, a non-dimensional parameter but usually the magnitude is specified in dB ($20log|S_{11}|$), for instance 0 dB indicates a magnitude $|S_{11}| = 1$ which means that all the radiation applied is reflected and it is the case for this specific resonator at all frequencies different to the 2.87 Gz. The phase in red and the magnitude in blue show the response as designed.

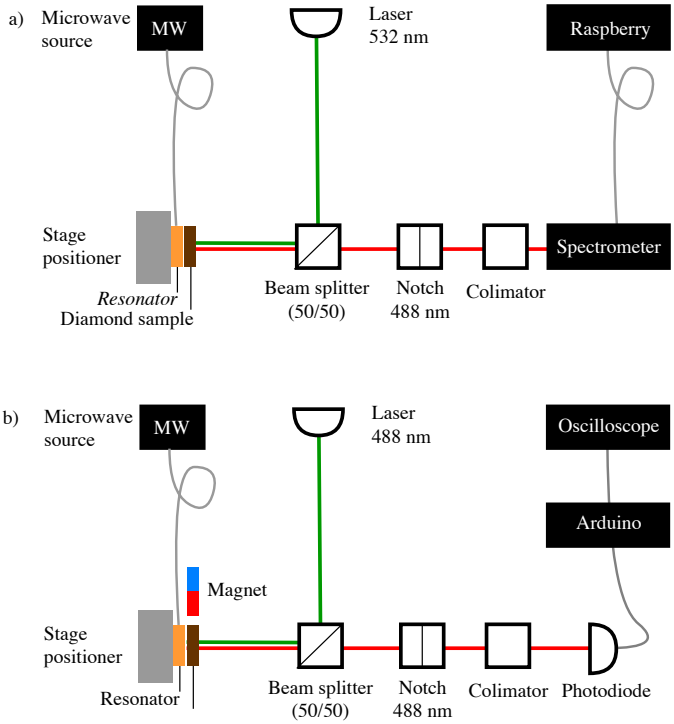

Figure III.4. a) Experimental measurement setup used to study the effect of the microwaves on the observed PL. The setup is simplified, the confocal microscope and other elements are replaced by the spectrometer and a Raspberry computer running a Python code to process and visualize the results. The microwave source and the resonator remain the same. b) Experimental and simplify setup adding a electromagnet and using a photodiode (AMS TSL257-LF Amplified Si PD) and a Portenta H7 Arduino board instead of the Spectrometer and the Raspberry. The microwave source, the resonator, laser and optical elements remain the same.

and shift of the levels appear due to electron spin-spin interaction [38]. Intersystem crossing (ISC), plays a key role in the excited state decay dynamics. It is the mechanism by which the center changes its spin state from excited state $m_s = \pm 1$ to the metastable $m_s = 0$.

Due to the higher ISC rate for the $m_s = \pm 1$ state under the laser light, the center is polarized to the $m_s = 0$ state, being the lifetime for the $m_s = 0$ excited state of 23 ns, almost double than the one corresponding to the $m_s = \pm 1$ excited state of 12.5 ns. The metastable state emits an infrared photon with a wavelength of 1046 nm and has a long lifetime of 300 ns, which is used to optically read the state of the center [39].

Considering the NV axis aligned with the Z-axis and an external magnetic field coupled to the center through the Zeeman effect, the triplet ground state has an effective spin Hamiltonian given by:

$$H_{nv} = DS_z^2 + \gamma_e B \cdot S$$

Where $D = 2.87$ GHz is the zero field splitting, S represents the electron spin projection operator, γ_e is the electron gyromagnetic ratio with a value of 28.0249 GHz/T, and B is the vector of the magnetic field.

The magnetic field vector component aligned with the NV^- axis couples with the center and then, the gap between the energies of the degenerated states, initially the same energy at zero field, now separates linearly with the magnetic field by $2\gamma_e B$ and therefore, the effect can be used to measure the external magnetic field strength because the splitting of the energy levels is directly proportional to the strength of the applied magnetic field component aligned with the NV axis, as shown in Figure III.6.

To continue the experiment, the experimental setup was extended by including an electromagnet placed close to the diamond Figure III.2. The electromagnet was connected to a precision power supply that allowed us to vary the voltage and thus the external magnetic field that acted on the material. Then the process consisted of taking measurements of the

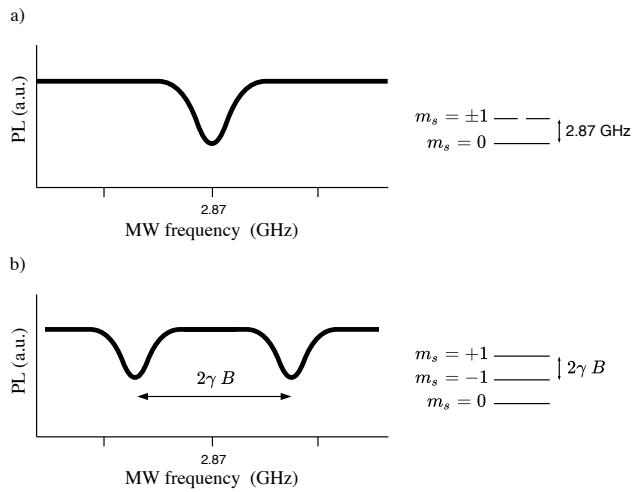

Figure III.5. Observed dip of the photoluminescence at the resonance frequency (a) and split of the degenerated state because of the Zeeman effect (b).

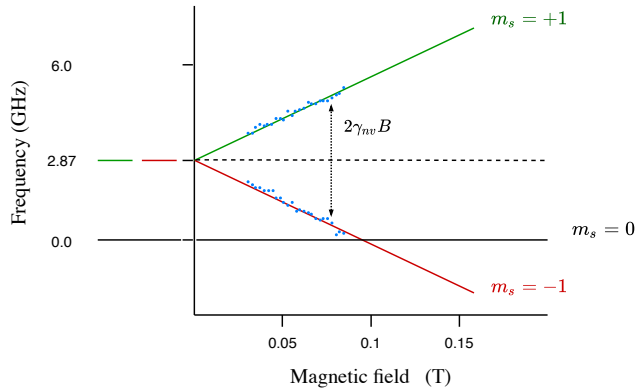

Figure III.6. Zeeman splitting of the degenerated state under the effect of an external magnetic field B and experimental results (blue dots). The energy splitting of the states $\mathrm{m_s} = +1$ and $\mathrm{m_s} = -1$ (green and red lines) is $2\gamma_\mathrm{e}\mathrm{B}$, linear and proportional to B with 2γ the gyromagnetic ratio of the NV center. The zero splitting happens at the resonance frequency of 2.87 GHz. When the magnetic field reaches $0.1\ T$ for the ground state and $0.05\ T$ for the excited state, then, due to the ground or excited state level anti-crossing, the $\mathrm{m_s} = 0$ and $\mathrm{m_s} = -1$ states become equal in energy.

observed PL for the different voltage values between 0 and 12 volts (Blue dots in Figure III.6).

Once demonstrated the control on the measurement of the magnetic field, it was possible to proceed with the steps towards improving the sensitivity and reduce the size of the device. For that purpose a new setup, more compact and simplified, was designed replacing the spectrometer by a photodiode connected to an Arduino board to read the signal and visualized it on an oscilloscope (Figure III.4-b).

With this new setup, it was possible to represent in more detail the PL landscape in proportion to the microwave frequency and the magnetic field, producing the series represented in the Figure III.7.

E. Visualizations

To more accurately measure the relationship between the magnetic field and the observed luminescence, the research team used a teslameter (FH-55 Teslameter [40]). The FH-55 tip probe was placed at the point where later would be placed the diamond, then, the value of the magnetic field, to the nearest hundredth of a millitesla, was recorded for each position of the magnet (moved at steps of $0.5\ mm$).

Once these measurements were collected, the study continued following the usual procedure, that is, first, shining with $532\ nm$ laser light to polarize the centers, leaving at least 30 minutes to ensure laser stabilization (otherwise the observed PL could be displaced, although it would not affect dips separation as a result of the splitting). Then, once the system stabilizes, was performed a frequency sweep from 2.7 to 3.0 GHz for each of the magnetic field values, corresponding to a specific position of the magnet with respect of the diamond.

Figure III.7 presents the results of the photoluminescence curves plotting intensity as a function of wavelength, Figure III.7a shows the magnetic resonance spectra of the ensemble of $\mathrm{NV^-}$centers corresponding to the 24 scans for different electromagnet voltage values between 0 and 12 volts, increasing 0.5 V at each step. In the figure, the darker the curve, the smaller the magnetic field. It can be seen how with the increase of the magnetic field the number of dips (corresponding to the transitions between the states $m_s = 0$ and $m_s = \pm 1$) increases due to how the different possible orientations of the NV axis within of the crystal structure perceive different projections of the magnetic field.

Figure III.7b presents also the PL as a function of the frequency for magnetic field values increasing at steps of $0.005\ mT$ from $0.23\ mT$ to $0.01\ mT$, in this case, the lighter the color of the curve, the lower the magnetic field.

In both cases the pattern is clear since it shows the expected symmetry as a consequence of the Zeeman splitting, the separation of the two global minima in the PL shows the linear dependence of the applied magnetic field and the distance between dips.

Finally, Figure III.8a and III.8b depicts the same data but in a 3D representation combining PL intensity, magnetic field and frequency.

IV. Conclusions

In a series of experiments, two samples of commercially available synthetic Ib diamonds from element6 vendor, a polycrystalline diamond and a single crystal, have been used. These samples were grown by the High Pressure High Temperature (HPHT) synthesis processes and characterized in a low vibration optical setup showing the characteristic spectra of an ensemble of the NV centers, both NV^0 and NV^-, as well as the side bands. The photoluminescence was represented as a function of wavelength as well as its evolution in time under different conditions.

Using the previous material, the research team has prepared an experimental setup in order to initialize the system, pump-

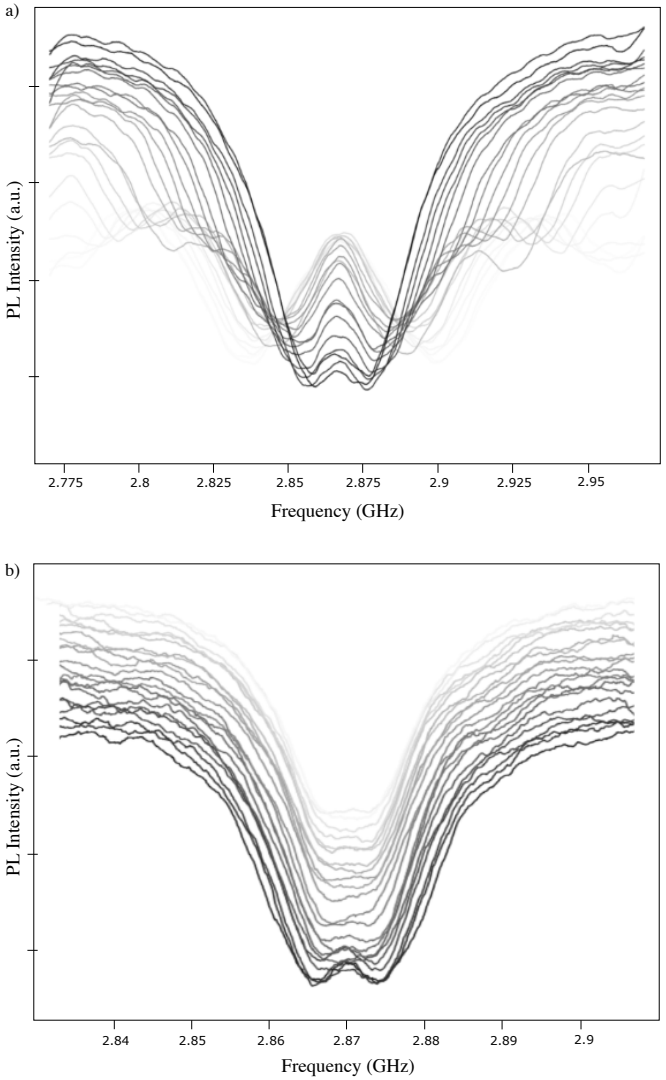

Figure III.7. Experimental measurement of photoluminescence as a function of the magnetic field for frequencies in the range of 2.7 to 3 GHz where it is observed how the gap between the resonance holes grows when the magnetic field increases. (a) is obtained using the described electromagnet changing the voltage and (b) is the result of the characterization moving the permanent magnet away at each step.

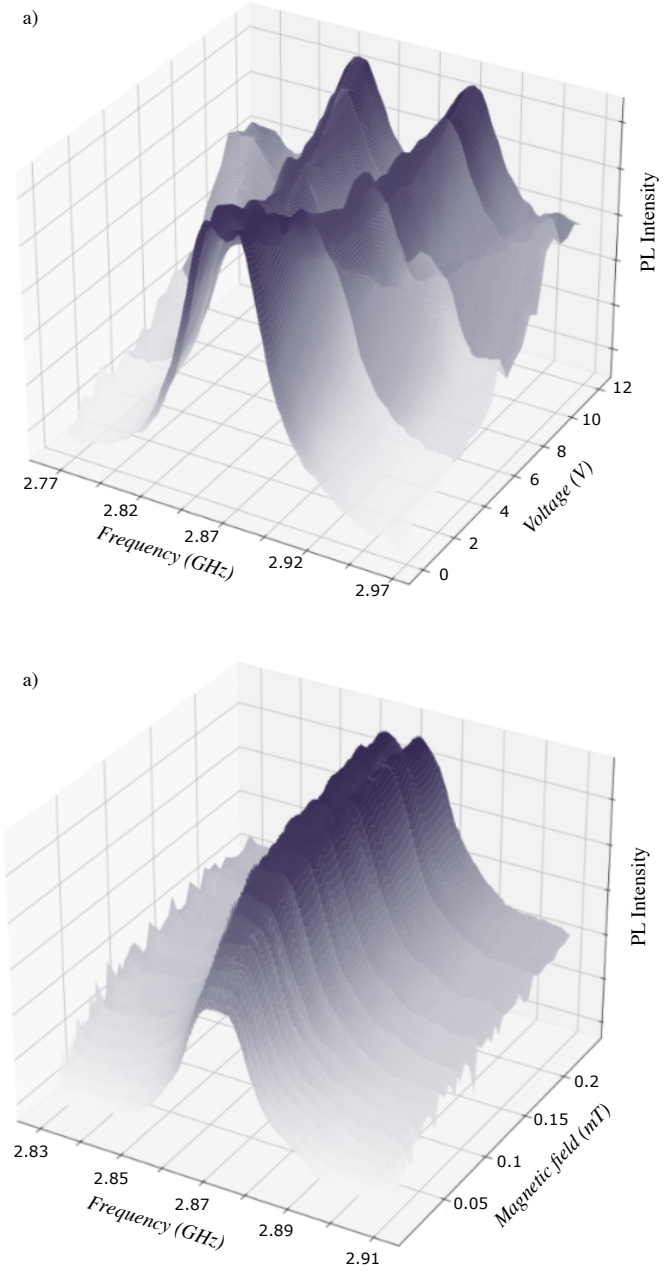

Figure III.8. Experimental measurement of photoluminescence as a function of the magnetic field for frequencies in the range of 2.7 to 3 GHz where it is observed how the gap between the resonance holes grows when the magnetic field increases. A 3D view, combining the three dimensions, photoluminescence, frequency and magnetic field. (a) is obtained using the described electromagnet changing the voltage and (b) is the result of the characterization moving the permanent magnet away at each step.

ing the electrons that form the color centers to the $m_s = 0$ state, by applying laser light, observing the expected behavior.

The development of a resonator, specifically designed to emit at the resonance frequency, has made it possible to apply a microwave pulse to the diamond under continuous laser illumination, this conditions have repopulated the degenerated states $m_s = \pm 1$ doing possible to observe the decrease in the observed PL. This happens due to the electrons follow the non-radiative decay path through the metastable state. The frequency sweep has verified the resonance frequency or energy gap between the states $m_s = 0$ and $m_s = \pm 1$. With this experimental setup, it has been possible, not just initialize the state but also identify the resonance frequency and verify the evolution of the PL when applying microwaves pulses, laying the groundwork for the next experiment.

In a last experiment, a magnetic field has been applied in a controlled way with the aim of measuring the displacement of the resonance frequencies due to the Zeeman effect and which constitutes the basis of magnetometry with color centers. The steps to develop this new setup as well as results are also part of this work leaving the way open to the miniaturization phase.

V. Acknowledgments

We thank M. A. Ramos, G. García, N. Gordillo and A. Redondo from CMAM (Centre for Micro Analysis of Materials) for fruitful discussions on diamond characteristics and its possible modification using ion irradiation in order to improve sensitivity. Dr. Matthew Markham from Element6 for providing the diamond samples. IMDEA Nanoscience nanofabrication facility, for assistance in many aspects, analysis of materials and fabrication of some of the components.

MICIN-AEI: Grants DETECTA ESP2017-86582-C4-3-R andEQC2018-005134-P

Comunidad de Madrid: Grant TEC2SPACE-CM P2018/NMT-4291

ONR-G: G#N62909-19-1-2053 (DEFROST),MADE-MICINN: PID2019-105552RB-C44

Garantía Juvenil nº201701520868, Comunidad de Madrid: G#2019-T2/IND-13367

References

[1] M. W. Doherty, N. B. Manson, P. Delaney, F. Jelezko, J. Wrachtrup, and L. C. Hollenberg, "The nitrogen-vacancy colour centre in diamond," *Physics Reports*, vol. 528, no. 1, pp. 1–45, 2013, the nitrogen-vacancy colour centre in diamond. [Online]. Available: https://www.sciencedirect.com/science/article/pii/S0370157313000562

[2] J. M. Taylor, P. Cappellaro, L. Childress, L. Jiang, D. Budker, and P. R. Hemmer, "High-sensitivity diamond magnetometer with nanoscale resolution," *Nature Physics*, vol. 4, no. 10, pp. 810–816, sep 2008. [Online]. Available: https://doi.org/10.1038%2Fnphys1075

[3] H. B. Dang, A. C. Maloof, and M. V. Romalis, "Ultrahigh sensitivity magnetic field and magnetization measurements with an atomic magnetometer," *Applied Physics Letters*, vol. 97, no. 15, p. 151110, 2010. [Online]. Available: https://doi.org/10.1063/1.3491215

[4] D. Drung, C. Assmann, J. Beyer, A. Kirste, M. Peters, F. Ruede, and T. Schurig, "Highly sensitive and easy-to-use squid sensors," *IEEE Transactions on Applied Superconductivity*, vol. 17, pp. 699–704, jun 2007. [Online]. Available: https://oadoi.org/10.1109/tasc.2007.897403

[5] M. Todaro, L. Sileo, and M. Vittorio, *Magnetic Field Sensors Based on Microelectromechanical Systems (MEMS) Technology*, 03 2012.

[6] C. Degen, M. Poggio, H. Mamin, C. Rettner, and D. Rugar, "Nanoscale magnetic resonance imaging," *Proceedings of the National Academy of Sciences of the United States of America*, vol. 106, pp. 1313–7, 02 2009.

[7] T. R. C. Amir Borna, "Non-invasive functional-brain-imaging with an opm-based magnetoencephalography system," Sandia National Laboratories, Albuquerque, NM, United States of America, Tech. Rep., 2020.

[8] M. Alkahtani and P. Hemmer, "Charge stability of nitrogen-vacancy color center in organic nanodiamonds," *Optical Materials Express*, vol. 10, 04 2020.

[9] N. Khaneja, "Squid magnetometers, josephson junctions, confinement and bcs theory of superconductivity," in *Magnetometers*, S. Curilef, Ed. Rijeka: IntechOpen, 2019, ch. 5. [Online]. Available: https://doi.org/10.5772/intechopen.83714

[10] T. Tierney, N. Holmes, and S. Mellor, "Optically pumped magnetometers: From quantum origins to multi-channel magnetoencephalography," *NeuroImage*, vol. 199, 12 2019.

[11] C. Degen, F. Reinhard, and P. Cappellaro, "Quantum sensing," *Reviews of Modern Physics*, vol. 89, no. 3, jul 2017. [Online]. Available: https://doi.org/10.1103%2Frevmodphys.89.035002

[12] J. Maze, P. Stanwix, J. Hodges, S. Hong, J. Taylor, and Cappellaro, "Nanoscale magnetic sensing with an individual electronic spin in diamond," *Nature*, vol. 455, pp. 644–7, 11 2008.

[13] L. Hall, G. Beart, E. Thomas, D. Simpson, and Mcguinness, "High spatial and temporal resolution wide-field imaging of neuron activity using quantum nv-diamond," *Scientific reports*, vol. 2, p. 401, 05 2012.

[14] T. Wolf, P. Neumann, K. Nakamura, H. Sumiya, T. Ohshima, J. Isoya, and J. Wrachtrup, "Subpicotesla diamond magnetometry," *Physical Review X*, vol. 5, no. 4, oct 2015. [Online]. Available: https://doi.org/10.1103%2Fphysrevx.5.041001

[15] M. W. Mitchell and S. P. Alvarez, "Quantum limits to the energy resolution of magnetic field sensors," *Reviews of Modern Physics*, vol. 92, no. 2, apr 2020. [Online]. Available: https://doi.org/10.1103%2Frevmodphys.92.021001

[16] N. B. M. Marcus W. Doherty, "The nitrogen-vacancy colour centre in diamond," School of Physics, University of Melbourne, VIC 3010, Australia, Tech. Rep., 2013.

[17] Wikipedia contributors, "Molecular symmetry Wikipedia, the free encyclopedia," 2022, [Online; accessed 23-May-2022]. [Online]. Available: https://en.wikipedia.org/w/index.php?title=Molecular_symmetry&oldid=1089050531

[18] J. Humphreys, Q. Liu, J. Humphreys, and R. Erne, *A Course in Group Theory*, ser. Oxford Graduate Texts in Mathematics. Oxford University Press, 1996. [Online]. Available: https://books.google.es/books?id=2jBqvVb0Q-AC

[19] A. M. Ferrari, M. D'Amore, K. E. El-Kelany, F. S. Gentile, and R. Dovesi, "The nv0 defects in diamond: A quantum mechanical characterization through its vibrational and electron paramagnetic resonance spectroscopies," *Journal of Physics and Chemistry of Solids*, vol. 160, p. 110304, 2022. [Online]. Available: https://www.sciencedirect.com/science/article/pii/S002236972100370X

[20] A. Gali, "Theory of the neutral nitrogen-vacancy center in diamond and its application to the realization of a qubit," *Phys. Rev. B*, vol. 79, p. 235210, Jun 2009.

[21] P. K. Kasper Jensen, "Magnetometry with nitrogen-vacancy centers in diamond," Niels Bohr Institute, University of Copenhagen, Denmark, Tech. Rep., 2017.

[22] E. van Oort and M. Glasbeek, "Cross-relaxation dynamics of optically excited nv centers in diamond," *Phys. Rev. B*, vol. 40, pp. 6509–6517, Oct 1989. [Online]. Available: https://link.aps.org/doi/10.1103/PhysRevB.40.6509

[23] W. C. Gaebel T., Domhan M., "Photochromism in single nitrogen-vacancy defect in diamond," *Applied Physics*, vol. 455, pp. 643–246, 2 2006. [Online]. Available: https://doi.org/10.1007/s00340-005-2056-2

[24] S. Choi, M. Jain, and S. Louie, "Mechanism for optical initialization of spin in nv center in diamond," *Phys. Rev. B*, vol. 86, 07 2012.

[25] S. A. L. J. Rogers, "New infrared emission of the nv centre in diamond: Zeeman and uniaxial stress studies," Laser Physics Center, Australian National University, Canberra, Tech. Rep., 2008.

[26] L. Robledo, H. Bernien, I. van Weperen, and R. Hanson, "Control and coherence of the optical transition of single nitrogen vacancy centers in diamond," *Phys. Rev. Lett.*, vol. 105, p. 177403, Oct 2010.

[27] S. D. Subedi, V. V. Fedorov, J. Peppers, D. V. Martyshkin, S. B. Mirov, L. Shao, and M. Loncar, "Laser spectroscopic characterization of negatively charged nitrogen-vacancy (nv−) centers in diamond," *Opt. Mater. Express*, vol. 9, no. 5, pp. 2076–2087, May 2019. [Online]. Available: http://opg.optica.org/ome/abstract.cfm?URI=ome-9-5-2076

[28] P. Neumann, R. Kolesov, V. Jacques, and J. Beck, "Excited-state spectroscopy of single NV defects in diamond using optically detected magnetic resonance," *New Journal of Physics*, vol. 11, no. 1, p. 013017, jan 2009. [Online]. Available: https://doi.org/10.1088/1367-2630/11/1/013017

[29] "element six. synthetic diamond and tungsten carbide experts," 2022, accessed: 2022-07-19. [Online]. Available: https://www.e6.com/

[30] V. S. Vavilov, "The properties of natural and synthetic diamond," *Physics-Uspekhi*, vol. 36, no. 11, pp. 1083–1084, nov 1993. [Online]. Available: https://doi.org/10.1070/pu1993v036n11abeh002207

[31] J. W. F. Jelezko, "Single defect centres in diamond: A review," DPhysikalisches Institut, UniversitÃ€t Stuttgart, Germany, Tech. Rep., 2006.

[32] L. Childress, M. G. Dutt, J. M. Taylor, A. S. Zibrov, and F. Jelezko, "Coherent dynamics of coupled electron and nuclear spin qubits in diamond," *Science*, vol. 314, pp. 281–285, 2006.

[33] S. D. Trofimov, S. A. Tarelkin, and S. V. Bolshedvorskii, "Spatially controlled fabrication of single nv centers in iia hpht diamond," *Opt. Mater. Express*, vol. 10, no. 1, pp. 198–207, Jan 2020. [Online]. Available: http://opg.optica.org/ome/abstract.cfm?URI=ome-10-1-198

[34] Q. L. Man Zhao, "Antenna for microwave manipulation of nv colour centres," The Institution of Engineering and Technology, Tech. Rep., 2020.

[35] K. S. Eisuke Abe, "Tutorial: Magnetic resonance with nitrogen-vacancy centers in diamond microwave engineering, materials science, and magnetometry," Spintronics Research Center, Keio University, Japan, Tech. Rep., 2018.

[36] "Voltera v-one pcb printer," 2022, accessed: 2022-07-24. [Online]. Available: https://www.voltera.io/store/v-one
[37] K. J. Maria Simanovskaia, "Sidebands in optically detected magnetic resonance signals of nitrogen vacancy centers in diamond," Department of Physics, University of California, Berkeley, Tech. Rep., 2013.
[38] J. Harrison, M. Sellars, and N. Manson, "Optical spin polarisation of the n-v centre in diamond," *Journal of Luminescence*, vol. 107, no. 1, pp. 245–248, 2004.
[39] L. Rogers, K. Jahnke, M. Metsch, A. Sipahigil, J. Binder, and Teraji, "All-optical initialization, readout, and coherent preparation of single silicon-vacancy spins in diamond," *Physical Review Letters*, vol. 113, 12 2014.
[40] "Magnetic field strength meter gauss-/teslameter fh 55," 2022, accessed: 2022-07-24. [Online]. Available: https://www.magnet-physik.de/upload/31925018-FH-55-e-3157.pdf
[41] K. Gilkes, S. Prawer, K. Nugent, J. Robertson, H. Sands, Y. Lifshitz, and X. Shi, "Direct quantitative detection of the sp3 bonding in diamond-like carbon films using ultraviolet and visible raman spectroscopy," *Journal of Applied Physics*, vol. 87, pp. 7283–7289, 05 2000.

APPENDIX
COMPONENT DETAIL

Figure A.1 shows the list of components.

Component	Supplier	Part Number	Price (USD)
Optical components			
Compact Laser Diode Module	Thorlabs	CPS532	$164.86
Argon Laser	Modu-Laser	Stellar Pro 488/50	$9815.00
Laser Line Filter	Thorlabs	FL488-10	$144.28
Long-Pass Dichroic Mirror	Semrock	LPD02-488RU	$630.00
Long-Pass Edge Filter	Semrock	LP02-488RU	$710.00
Plano-Convex Lens	Thorlabs	LA1027 N-BK7	$22.34
Objective 20x/0.35	Olympus	SLMPlan	$1050.00
Beam Splitter (50/50)	Thorlabs	BSW26R	$295.21
Beam Splitter (90/10)	Thorlabs	-	$178.00
Electronic components			
Dual SMU System	Keithley	2614B	-
Portenta H7	Arduino	ABX00042	$99.00
Raspberry Pi	Raspberry Pi	3 Model B+	$35.00
Oscilloscope	Tektronics	TBS1202B	$1509.53
Spectrometer	Andor	Shamrock 500i	-
CCD Camera	Thorlabs	DCC1645C-HQ	-
Amplified Si Phtodiode	Texas Instruments	TSL257-LF	$2.09
Teslameter FH55	MAGNET-PHYSIK	2000550EBA01	-
Microwave Source	Rohde & Schwarz	SMC100 A	-
Spectrometer	Ocean Optics	AVS USB2000	-
Electromagnet	RS PRO	7393264	$14.15
Structural components			
XYZ Positioner	Thorlabs	LNR50M	3x$946.00
Base Plate	Thorlabs	LNR50P1	$74.54
Right-Angle Bracket	Thorlabs	LNR50P2	$114.64
Optical Post x5	Thorlabs	TR20/M-P5	$21.30
Samples			
Polycrystaline diamond	Element Six	LNR50M	-
Single crystal diamond	Element Six	LNR50P1	-

Figure A.1. List of components

APPENDIX
CHARACTERIZATION DETAILS

Figure A.1 shows the photoluminescence spectra for an NV spin ensemble embedded in a single crystal diamond (red) and a polycrystalline diamond (blue). The typical luminescence curve representing the intensity as a function of the wavelength with the zero phonon lines (ZPL) and the phonon sidebands. NV^- and NV^0 can be optically distinguished by their different zero phonon lines at $639\,\mathrm{nm}$ and $575\ \mathrm{nm}$ respectively. The NV^- zero-phonon line is determined by the intrinsic difference in energy levels between spin triplet ground and excited states. The NV^- phonon sideband is shifted to a higher frequency in absorption and to a lower frequency in fluorescence.

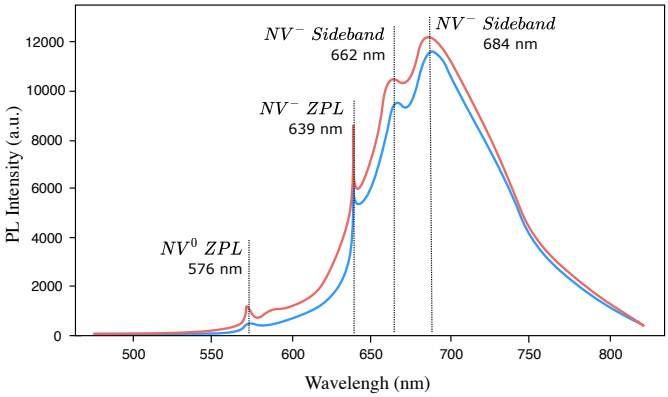

Figure A.1. Photoluminescence spectra for an NV spin ensemble .

The two samples were characterized at room temperature under different conditions of laser light intensities and at different depths of focus getting almost identical results. Specifically, Figure A.2a shows the luminescence curve plotting intensity as a function of wavelength for the diamond single crystal.

In the setup, the objective can be translated upward or downward changing the focus. The lines represent the spectra measured directly with focus on the surface (green), and the rest of the lines in blue, orange, red and gray, those measured focusing at the different depths, that is, $4\ \mu m$, $8\ \mu m$, $12\ \mu m$ and $16\ \mu m$, all of them very similar. The greater the depth, the greater the observed intensity of the luminescence due to the volume of the stimulated material is greater and therefore, so is the number of activated centers. As a consequence, the number of emitted photons increases.

Similarly Figure A.2b shows the luminescence curve plotting intensity as a function of wavelength for the diamond single crystal but in this case the lines represent the spectra measured for different laser intensities: $20\ \mu W$ (green line), $40\ \mu W$ (blue), $60\ \mu W$ (orange), $75\ \mu W$ (red) and $80\ \mu W$ (grey). In general, the greater the laser power, the greater the observed intensity of the luminescence because of the linearity between laser intensity and PL.

Figure A.2c and Figure A.2d show results for the diamond polycrystalline sample, very similar to the ones from the single-crystal diamond.

Finally, Figure A.2e and Figure A.2f show the zoom in the frequency range from $480\ nm$ to $550\ nm$ for the single-crystal and polycrystalline samples respectively. In both cases a small Raman peak corresponding to the vibration of the $sp3$ diamond lattice [41] was observed at $523\ nm$ or $1371\ cm^{-1}$.

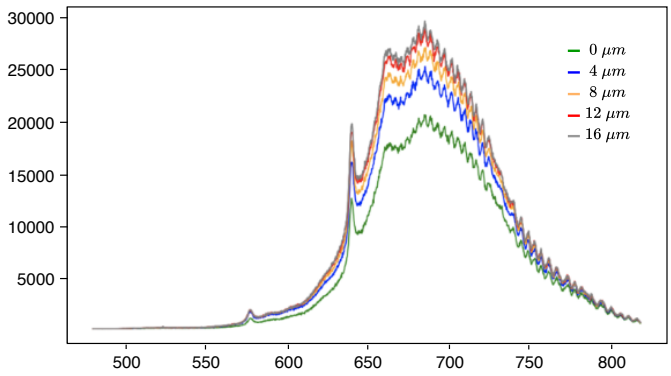

a) Single Crystal. Laser power set at 40 μWatts

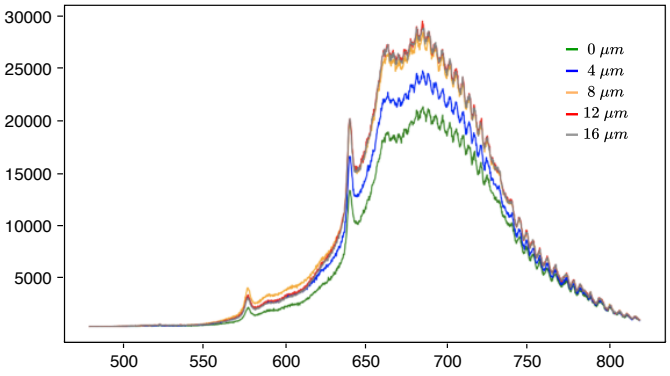

a) Polycrystal. Laser power set at 40 μWatts

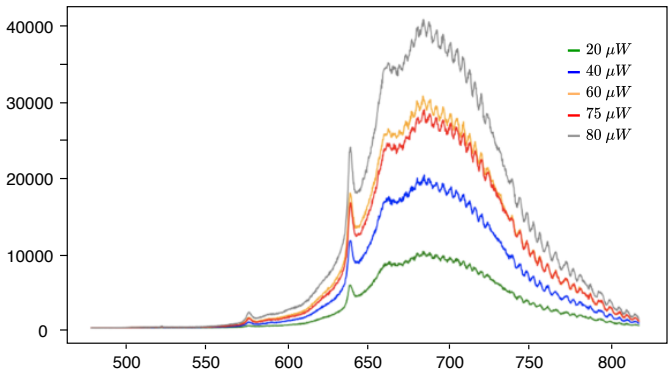

b) Single Crystal. Laser focused on the surface plane

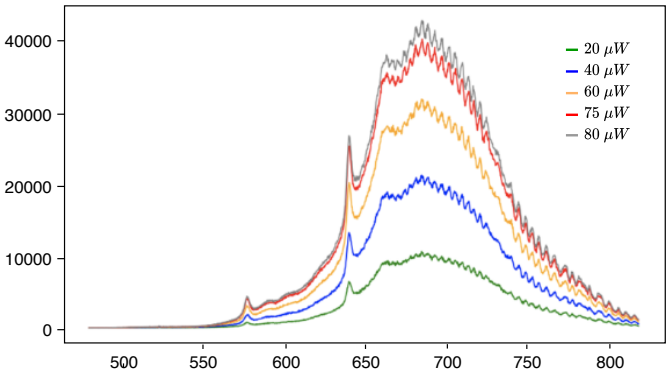

b) Polycrystal. Laser focused on the surface plane

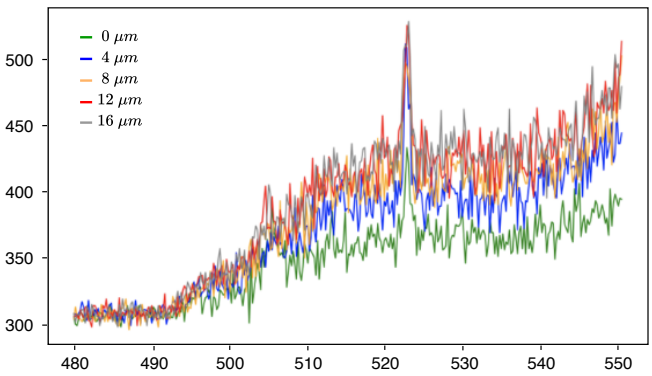

c) Single Crystal. Laser power set at 40 μWatts. Raman peak

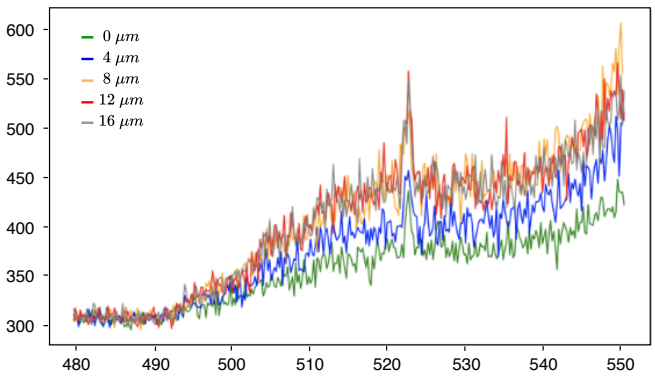

c) Polycrystal. Laser power set at 40 μWatts. Raman peak

Figure A.2. Photoluminescence spectra for the single crystal (a and b) and detail of the observed Raman peak (c).

Figure A.3. Photoluminescence spectra for the polycrystalline sample (a and b) and detail of the observed Raman peak (c).